Upregulated expression of ubiquitin ligase TRIM21 promotes PKM2 nuclear translocation and astrocyte activation in experimental autoimmune encephalomyelitis

Luting Yang[1,#], Chunqing Hu[1,#], Xiaowen Chen[1,#], Jie Zhang[1,#], Zhe Feng[1], Yanxin Xiao[1], Weitai He[1], Tingting Cui[1], Xin Zhang[1], Yang Yang[1], Yaling Zhang[1], Yaping Yan[1,*]

Short running title: TRIM21 promotes PKM2 nuclear translocation in astrocytes of EAE

1: Key Laboratory of the Ministry of Education for Medicinal Resources and Natural Pharmaceutical Chemistry, National Engineering Laboratory for Resource Development of Endangered Crude Drugs in Northwest of China, College of Life Sciences, Shaanxi Normal University, Xi'an, 710119, China

#: These authors contributed equally to this work.

*Corresponding author: Yaping Yan, E-mail: yaping.yan@snnu.edu.cn

Abstract

Reactive astrocytes play critical roles in the occurrence of various neurological diseases such as multiple sclerosis. Activation of astrocytes is often accompanied by a glycolysis-dominant metabolic switch. However, the role and molecular mechanism of metabolic reprogramming in activation of astrocytes have not been clarified. Here, we found that PKM2, a notoriously known rate-limiting enzyme of glycolysis, displayed nuclear translocation in astrocytes of EAE (experimental autoimmune encephalomyelitis) mice, an animal model of multiple sclerosis. Prevention of PKM2 nuclear import by DASA-58 significantly reduced the activation of primary astrocytes, which was observed by decreased proliferation, glycolysis and secretion of inflammatory cytokines. Most importantly, we identified the ubiquitination-mediated regulation of PKM2 nuclear import by ubiquitin ligase TRIM21. TRIM21 interacted with PKM2, promoted its nuclear translocation and stimulated its nuclear activity to phosphorylate STAT3, NF-κB and interact with c-myc. Further single-cell RNA sequencing and immunofluorescence staining demonstrated that TRIM21 expression was upregulated in astrocytes of EAE. TRIM21 overexpressing in primary astrocytes enhanced PKM2-dependent glycolysis and proliferation, which could be reversed by DASA-58. Moreover, intracerebroventricular injection of a lentiviral vector to knockdown TRIM21 in astrocytes or intraperitoneal injection of TEPP-46, which inhibit the nuclear translocation of PKM2, effectively decreased disease severity, CNS inflammation and demyelination in EAE. Collectively, our study provides novel insights into the pathological function of nuclear glycolytic enzyme PKM2 and ubiquitination-mediated regulatory mechanism that are involved in astrocyte activation. Targeting this axis may be a potential therapeutic strategy for the treatment of astrocyte-involved neurological disease.

Keyword:

Pyruvate kinase M2, astrocyte, TRIM21, experimental autoimmune encephalomyelitis, ubiquitination

Introduction

Multiple sclerosis (MS) is a chronic inflammatory disease of the central nervous system (CNS), which accounts for the leading cause of neurological disability in young adults. The hallmarks of this disease is varied and complex, ranging from astrocyte proliferation, microglia activation, neuroinflammation and damage to myelin sheaths (Kuhlmann et al., 2023). Accumulating evidence suggests the critical roles of neurons in MS pathology. However, with the deepening of research, local glia cells have been shown to potentiate inflammation and lead to neurodegeneration, among which astrocytes have attracted much attention with their diverse functions (Lee et al., 2023).

Astrocytes are the most abundant type of glia cells and provide physical, structural and metabolic support for neurons. Astrocytes respond to CNS diseases through a process of activation that encompasses cell proliferation, morphological, molecular and functional modifications. This phenomenon, also termed reactive astrocyte or astrogliosis, results in loss of brain homeostatic functions and leads to the occurrence of neurological and neuropsychiatric disorders (Verkhratsky et al., 2023). The presence of activated astrocytes which is evidenced by increased GFAP staining, was found before immune cell infiltration in MS and its animal model, EAE (Correale and Farez, 2015). Several lines of evidence bolster the conception that activated astrocytes are considered to be early events and contributors to lesion development in MS and EAE etiopathology (das Neves et al., 2021). With the accepted notion of astrocyte contributions to MS or EAE, mounting interest has been focused on dissecting how astrocytes are reactive.

Activated immune cells, like cancer cells, require higher biosynthetic and energy needs for immune response, proliferation and survival. This involves reprogramming of their metabolic pathways. Proinflammatory immune cells, including reactive astrocytes, usually undergo a metabolic switch from oxidative phosphorylation to Warburg-type glucose metabolism (Vaupel and Multhoff, 2021, Xiong et al., 2022). Moreover, elevated level of aerobic glycolysis have been characterized in astrocyte of MS patients (Afzal et al., 2020, Nijland et al., 2015). Elevated glycolysis is crucial for

sustaining astrocyte proliferation, the secretion of proinflammatory cytokines and neurotrophic factors and subsequent neuronal loss in the CNS. As such, deciphering glycolysis-dominant metabolic switch in astrocytes is the basis for understanding astrogliosis and the development of neurological diseases such as multiple sclerosis.

Pyruvate kinase M2 (PKM2), a rate-limiting enzyme of glycolysis, is a key molecule that governs aerobic glycolysis. Low glycolytic enzyme activity of PKM2 promotes the conversion of pyruvate to lactate, which leads to aerobic glycolysis (Lee et al., 2022). In the cytoplasm, PKM2 exists in tetrameric form and possesses high pyruvate kinase activity. Specifically, PKM2 can translocate to the nucleus in its dimeric form. With a low-glycolytic function, nuclear PKM2 can act as a protein kinase or transcriptional coactivator to regulate proliferation, inflammation and metabolic reprogramming of cells (Liu et al., 2022). The overexpression and nuclear translocation of PKM2 have been well documented in CNS disease. Moreover, nuclear PKM2 was upregulated in neutrophils and macrophages in patients with ischemic stroke (Dhanesha and Patel, 2022, Li et al., 2022). Nuclear PKM2 in neurons was shown to promote neuronal loss in Alzheimer's disease (Traxler et al., 2022), suggesting that PKM2 is a key player in the development of neurological disease. Although previous studies have suggested that PKM2 could regulate astrocyte proliferation (Zhang et al., 2015), its potential function in astrocyte metabolic reprogramming and the upstream mechanisms underlying PKM2 nucleocytoplasmic shuttling are still elusive.

In this report, we identified TRIM21 as the interacting protein of PKM2 and found that TRIM21 promoted the nuclear translocation of PKM2, thus contributing to astrocyte glycolysis and proliferation in EAE. Most importantly, we used the EAE model to demonstrate that targeting TRIM21-PKM2 axis alleviated the disease process.

Our finding might help to understand the mechanism underlying astrocyte activation in neurological diseases and provide therapeutic target for the treatment of multiple sclerosis.

Results

Identification of PKM2 nuclear translocation in astrocytes during EAE

To investigate whether PKM2 repositioning or aberrant expression drives astrocyte dysfunction in EAE mice, we obtained tissue samples from the spinal cords of different phases of EAE and control mice. Nuclear translocation of PKM2 was initially observed at the onset phase, which sustained to the peak and chronic phases of the disease. Compared to the cytoplasmic localization of PKM2 in control mice, the expression level of PKM2 was elevated in different phases of EAE (Fig. 1A). MOG_{35-55}-stimulated splenocytes from EAE mice were previously shown to mimic MS pathology and are frequently used as an in vitro autoimmune model to investigate MS and EAE pathophysiology (Chen et al., 2009, Kozela et al., 2015). To validate the expression pattern of PKM2 in astrocytes *in vitro*, primary astrocytes were isolated and cultured with supernatants from MOG_{35-55}-stimulated splenocytes (MOG_{sup}) of EAE. Activated astrocytes were observed following co-culture with the above-mentioned supernatant, showing obviously increased expression of GFAP, a marker of reactive astrocytes (Fig. 1B). Consistently, compared with those in control astrocytes, nuclear ratio and expression of PKM2 were significantly greater in MOG_{sup}-stimulated astrocytes (Fig. 1C and D). Together, these data demonstrated the nuclear translocation of PKM2 in astrocytes from EAE mice.

Prevention of PKM2 nuclear transport suppresses aerobic glycolysis and proliferation in astrocytes

Metabolic switch of astrocytes to aerobic glycolysis and proliferation of astrocytes are early events in MS and EAE. To explore the contribution of PKM2 nuclear translocation to the alternation of astrocyte metabolism and function, DASA-58, the inhibitor of PKM2 nuclear transport that favors its tetramerization was used. Pretreatment with DASA-58 effectively reduced the nuclear ratio of PKM2 in MOG_{sup} stimulated astrocytes (Fig. 2A and B). As expected, MOG_{sup} stimulation,

177 which mimics the autoimmune response in MS patients, induced an increase in the
178 glycolytic activity of astrocytes, as evidenced by glucose consumption and lactate
179 production. However, these effects were significantly counteracted by DASA-58
180 treatment (Fig. 2C). To further confirm these result, glycolysis-related enzymes and
181 transcription factors including LDHA, PKM2 and c-myc were examined. Among
182 these proteins, DASA-58 pretreatment severely impaired the upregulation of
183 phosphorylated c-myc induced by MOG_{sup} stimulation (Fig. 2D).

184 To determine whether DASA-58 could alter astrocyte proliferation, CCK-8 and
185 EdU assays were performed. Figure 2E showed that treatment with 25 μM and 50 μM
186 DASA-58 impaired the proliferation of astrocytes, and 50 μM owned better effect.
187 Additionally, EdU incorporation assays showed that 50 μM DASA-58 mostly
188 abrogated the MOG_{sup}-induced astrocyte proliferation (Fig. 2F and G). In addition,
189 DASA-58 pretreatment reduced the expression of inflammatory cytokines including
190 IL-6, TNF-α and iNOS in MOG_{sup}-stimulated astrocytes (Fig. S1). From the above
191 results we can conclude that abrogation of PKM2 nuclear transport can markedly
192 decrease the proliferation and glycolysis of astrocytes.

193 **Nuclear PKM2 promotes the activation of NF-κB and STAT3 pathways**

194 Upon nuclear translocation, PKM2 acquires protein kinase and transcriptional
195 coactivator activities. As nuclear PKM2 has been reported to interact with STAT3 and
196 NF-κB, which are dominant signaling pathways involved in orchestrating cell
197 proliferation, inflammation and glycolysis, we were curious to investigate whether
198 nuclear PKM2 regulates the activation of these two pathways. The activation of
199 STAT3 and NF-κB requires two critical steps: phosphorylation of key components,
200 nuclear translocation and retention of STAT3 or p65/p50 subunits. As expected,
201 DASA-58 pretreatment partially attenuated the phosphorylation of STAT3 and NF-κB
202 pathways following MOG_{sup} stimulation (Fig. 3A-C). Phosphorylation only
203 contributes to the transient activation of STAT3 and NF-κB, and constant activation
204 also requires the nuclear retention of STAT3 and p50/p65. To test our hypothesis that
205 nuclear PKM2 might promote the retention of p50/p65 and STAT3, we purified
206 nuclear and cytoplasmic proteins. Western blotting assays showed that inhibiting

PKM2 nuclear localization with DASA-58 suppressed the nuclear retention of p50/p65 and STAT3 (Fig. 3D).

To further clarify the mechanism by which PKM2 regulated the nuclear retention of STAT3 and NF-κB, immunoprecipitation was performed. The results verified that endogenous PKM2 could directly bind to NF-κB subunits p50/p65 and STAT3 in astrocytes (Fig. 3E). Therefore, nuclear PKM2 interacts with p50/p65 and STAT3, favoring their nuclear retention and constant activation of NF-κB and STAT3 pathways.

E3 ligase TRIM21 interacts with PKM2 in astrocytes

With deepening of the research, amounting evidences support that post-translational modifications (PTMs), representing by ubiquitination, acetylation, sumoylation and phosphorylation are major mechanisms to regulate the process of PKM2 nuclear translocation. To illustrate underlying mechanism accounting for nuclear translocation of PKM2 in astrocytes, mass spectrometry combined with immunoprecipitation of PKM2 were performed. Several enzymes involved in glycolysis and gluconeogenesis including ENO1, ALDOA, MDH2, LDHA and LDHC were identified to be interacted with PKM2 (Fig. 4A). Analysis of biological processes according to Gene Ontology (GO) terms confirmed that the binding proteins of PKM2 are enriched in metabolic processes (Fig. 4B). Moreover, the results of KEGG and Wikipathway enrichment analysis indicate that PKM2-interacting proteins were enriched in glycolysis, glucogeogenesis and NF-κB pathway (Fig. 4C and 4D). Amongst these potential interacting proteins, the most attracting one is TRIM21, an E3 ligase involved in the process of ubiquitination (Fig. 4A). Coincidentally, we previously reported the proinflammatory role of TRIM21 in keratinocytes by ubiquitylating the p50/p65 subunits of NF-κB(Yang et al., 2021). We were curious to verify whether TRIM21 interacted with and regulated the subcellular localization of PKM2 in astrocytes. Molecular docking revealed a strong binding affinity between PKM2 and TRIM21 (Fig. 4E, left). TRIM21 is bound to PKM2 via hydrogen bonds between the amino acids of the two molecules (Fig. 4E, right). By immunoprecipitation assays, we demonstrated the endogenous binding of PKM2 with

TRIM21 in primary astrocytes (Fig. 4F). To further confirm the results of PKM2-TRIM21 interaction, plasmids of Myc-tagged TRIM21 and Flag-tagged PKM2 were constructed. Reciprocal immunoprecipitation with either Myc or Flag antibodies verified exogenous binding between PKM2 and TRIM21 (Fig. 4G and 4H). To map the binding domains between PKM2 and TRIM21, a series of truncation with deletion (Δ) of various domains of TRIM21 and PKM2 were constructed. The deletion of C-terminal PRY-SPRY domain abolished the binding between TRIM21 to PKM2, which indicated that PRY-SPRY domain of TRIM21 was responsible for the interaction with PKM2 (Fig. 4I). However, the deletion of either N- or C-terminal of PKM2 did not affect the binding between TRIM21 to PKM2, indicating that AB domain (44 to 388 amino acids) of PKM2 might interact with TRIM21 (Fig. 4J).

Upregulated TRIM21 expression in astrocytes of EAE mice and in activated primary astrocytes

Previous studies have documented upregulated expression of TRIM21 in various types of cancers. Moreover, our previous study is the first to uncover the upregulation of TRIM21 in the epidermis of psoriatic patients, an autoimmune skin disease characterized by hyperproliferation of epidermal keratinocytes (Yang et al., 2018, Yang et al., 2021). To determine the relative expression of TRIM21 in astrocytes of EAE mice, we firstly performed single-cell RNA sequencing (scRNA-seq) on brain samples from the control, EAE peak and chronic stages. ScRNA-seq analysis revealed differential expression of TRIM21 in multiple cell populations. Compared to that in other cell types, TRIM21 expression in astrocytes was relatively high (Fig. 5A). We identified 12 astrocyte subpopulations, whereas TRIM21 expression was divergent in different astrocyte clusters (Fig. 5B-5C). Most importantly, TRIM21 expression was augmented in astrocytes in both peak and chronic phases of EAE compared to that in control mice (Fig. 5D). Consistently, bioinformatic analysis of the GEO database (GSE136358) revealed significant elevation of TRIM21 expression in astrocytes at the onset, peak and chronic phases of EAE disease (Fig. 5E).

To further confirm the results of TRIM21 expression from scRNA-seq and GEO datasets, activated astrocytes were mimicked by stimulating primary astrocytes with

267 MOG_{sup}. Compared to those in non-stimulated astrocytes, qPCR and western blotting
268 analysis revealed dramatic increases in TRIM21 mRNA and protein expression in
269 activated astrocytes (Fig. 5F and 5G). Moreover, immunofluorescence staining further
270 demonstrated that TRIM21 expression was greater in astrocytes from EAE mice when
271 compared with control mice (Fig. 5H). Taken together, our results uncover the
272 upregulated expression of TRIM21 in astrocytes of EAE mice, which imply that the
273 ectopic expression of this ubiquitin ligase TRIM21 might be a potent regulator of
274 PKM2 repositioning in the nucleus.

275 **TRIM21 ubiquitylates and promotes the nuclear translocation of PKM2**

276 Ubiquitination is endowed with multifaceted function to regulate degradation,
277 localization and activation of substrate proteins. As PKM2 has been demonstrated to
278 be the interacting protein and substrate of TRIM21, we next examined the impact of
279 TRIM21 on PKM2 localization. Overexpression of TRIM21 induced a robust increase
280 in the nuclear ratio of PKM2 (Fig. 6A, Fig. S2A). In contrast, knockdown of TRIM21
281 led to a reduction in the nuclear ratio of PKM2 (Fig. 6B, Fig. S2B). To a greater
282 extent, TRIM21 was found to be a potent driver of PKM2 translocation in astrocytes
283 of EAE. To deeply unveil the mechanism of TRIM21-mediated binding with PKM2,
284 the ubiquitination linkage type was investigated. In addition to K48-linked
285 ubiquitination, which directs proteins for degradation, K63-linked ubiquitination is
286 implicated in the regulation of protein localization and activation.
287 Immunoprecipitation implied that K63-linked ubiquitination of PKM2 was enhanced
288 upon overexpression of TRIM21 (Fig. 6C). Collectively, the data showed that
289 TRIM21 promoted K63-linked ubiquitination of PKM2 and facilitated its nuclear
290 translocation in astrocytes.

291 **TRIM21 promotes aerobic glycolysis and proliferation by enhancing PKM2**
292 **nuclear function in astrocytes**

293 As TRIM21 promoted the nuclear translocation of PKM2, we explored the impact
294 of TRIM21 on the nuclear function of PKM2. Our results showed that the levels of
295 phosphorylated STAT3 and p65 were significantly increased upon TRIM21
296 overexpression (Fig. 6D). We next examined whether TRIM21 could affect the

297 binding of PKM2 to c-myc, STAT3 and NF-κB subunits. As shown in Figure 6E,
298 overexpression of TRIM21 promoted the binding of PKM2 to c-myc, STAT3 and p50
299 subunit of NF-κB. Nuclear PKM2 contributed to nuclear retention of STAT3 and
300 NF-κB, which retained the constant activation of these two signaling pathways. We
301 were curious to investigate whether TRIM21 is involved in this process. Notably,
302 fractionation analysis revealed that overexpression of TRIM21 increased the nuclear
303 accumulation of c-myc, STAT3 and p50/p65 subunits. Conversely, pretreatment with
304 DASA-58, which abrogated the nuclear translocation of PKM2, diminished the
305 nuclear retention of the aforementioned transcription factors (Fig. 6F). These findings
306 revealed that the TRIM21-mediated nuclear translocation of PKM2 promoted its
307 nuclear function.

308 To further assess the functional consequences of TRIM21-mediated nuclear
309 translocation of PKM2, the glycolytic activity and proliferation of astrocytes were
310 measured. As shown in Figure 6G, TRIM21 overexpression increased the ratio of
311 EdU positive cells. However, the increase in astrocyte proliferation caused by
312 TRIM21 upregulation was significantly antagonized by the DASA-58 treatment (Fig.
313 6G). Similarly, upregulated TRIM21 promoted lactate production and glucose
314 consumption, which were reversed by DASA-58 (Fig. 6H). In summary, our results
315 indicate that nuclear PKM2-mediated metabolic reprogramming is crucial for
316 TRIM21-stimulated proliferation of astrocytes.

317 **TRIM21 knockdown in astrocyte or TEPP-46 treatment inhibits the**
318 **development of EAE**

319 To determine the therapeutic effect of TRIM21 knockdown in astrocytes on EAE,
320 shTRIM21 and control lentivirus were given to mice by intracerebroventricular
321 administration at disease onset (15 days post immunization). As expected, shTRIM21
322 treatment suppressed disease severity of EAE. At the end time point at day 22 p.i.,
323 shTRIM21-treated group showed reduced disease scores, although no statistical
324 difference was observed compared to control group (Fig. 7A). To further measure the
325 effect of TRIM21 knockdown in astrocytes on pathological changes in EAE mice, HE
326 and LFB staining were performed. As expected, inflammation and demyelination

were less pronounced in shTRIM21-treated group (Fig. 7B and 7C). Staining for TRIM21 showed that TRIM21 expression was reduced in astrocytes after intracerebroventricular injection of shTRIM21 lentivirus (Fig. 7D). Demyelination lesions were also evaluated by myelin basic protein (MBP) staining. Knockdown of TRIM21 in astrocytes significantly increased MBP positive areas, which indicated the inhibited demyelination in shTRIM21-treated group compared with control group (Fig. 7E). In EAE, microglia and astrocyte activation are linked with demyelination, we next stained GFAP and IBA1 to measure the activation of astrocytes and microglia. Knocking down TRIM21 in astrocytes decreased GFAP expression on spinal cord sections. The decrease of $GFAP^+$ cell numbers was observed in both gray and white matter from shTRIM21-treated mice (Fig. 7F). For activated microglia expressing IBA1, similar results were observed. Control group showed a widespread activation, while shTRIM21-treated group showed a significant decrease in IBA1 positive cells in both white matter and gray matter of spinal cord (Fig. 7G).

Therapeutic potential of PKM2 nuclear translocation inhibition with TEPP-46 was also tested in the EAE model. TEPP-46 is an allosteric activator that blocks the nuclear translocation of PKM2 by promoting its tetramerization. Intraperitoneal treatment with TEPP-46 during prevention stage resulted in decreased disease severity (Fig. S3A). TEPP-46-treated mice exhibited reduced inflammation and demyelination (Fig. S3B-S3E). The activation of GFAP positive astrocytes and IBA1 positive microglia were correspondingly reduced in TEPP-46-treated mice (Fig. S3D and S3E). Taken together, these results showed that TRIM21 deficiency in astrocytes or prevention of PKM2 nuclear translocation substantially inhibited inflammation and myelin depletion in EAE mice.

Discussion

Reactive astrocytes, or astrocyte activation are recognized as common feathers of CNS pathology, including neurodegenerative and demyelinating diseases (Patani et al., 2023). Preferential metabolic switch toward aerobic glycolysis favors astrocyte transfer from “resting” to “reactive” state. Thus, deciphering the mechanism responsible for astrocyte metabolic switch in response to neurological disease will provide new insights and new therapeutic targets for CNS diseases. Previous studies have detected nuclear translocation of PKM2 in astrocytes after spinal cord injury (Zhang et al., 2015) and in a chronic inflammatory pain model (Wei et al., 2020), in which the regulatory effect of PKM2 on aerobic glycolysis and proliferation has been indicated. However, in EAE model of multiple sclerosis, whether PKM2 nuclear translocation can be observed in astrocytes and the causal mechanisms involved are still unclarified. To the best of our knowledge, this study is the first to document the nuclear translocation of PKM2 in astrocytes of EAE. Furthermore, we clarified a ubiquitination-mediated regulation of PKM2 nuclear transport. Our newly identified upregulated expression of E3 ubiquitin ligase TRIM21 in astrocytes from EAE mice promotes the nuclear translocation of PKM2 to further activate astrocytes (Fig. 8).

Among the PTMs that regulate expression and localization of PKM2, phosphorylation is the most frequently reported type, it remains less well known whether ubiquitination could be a potential player. Ubiquitin-mediated degradation of PKM2 has been reported. Recently, in ovarian cancer, E3 ligase CHIP was shown to directly interact with PKM2 and mediate its degradation (Shang et al., 2017). TRIM family E3 ligase TRIM35 was previously shown to mediate the degradation of PKM2 in cardiomyocytes and breast cancer cells (Lorenzana-Carrillo et al., 2022, Wu et al.,

2022). Although laforin/malin E3 ligase-induced ubiquitination of PKM2 did not lead to its degradation, ubiquitination in this case impaired its nuclear transport (Viana et al., 2015). Different from these findings, it should be emphasized that our study adds to the current knowledge that ubiquitination, in addition to SUMOylation (Zhou et al., 2022) and phosphorylation (Yang et al., 2012), could induce the relocalization of PKM2 in the nucleus.

TRIM21 is found in our study to interact with and ubiquitylate PKM2. As a traditional E3 ubiquitin ligase, multiple key molecules involved in metabolism, immunity and inflammation have been recognized as substrates of TRIM21 (Chen et al., 2022). In addition to the well-known function of TRIM21 in inflammation, an increasing number of studies have suggested that TRIM21 plays a regulatory role in glucose metabolism. Glycolytic-related enzymes including PFK1 (Tang et al., 2022), GLUT1 (Gu et al., 2022) and glycolysis-related transcription factor HIF-1α (Chen et al., 2021) were identified to be substrates of TRIM21, and TRIM21 mediated the ubiquitin-dependent degradation of these proteins, thereby inhibiting aerobic glycolysis. Hereby, we recognized PKM2 as a substrate of TRIM21. The fate of the ubiquitinated protein varies greatly, depending on the linkage type present in the ubiquitin chain. Here, we found that TRIM21 promoted K63-linked ubiquitination of PKM2, the second common type of linkage that is typically not associated with protein degradation. These findings imply that enzymes and proteins implicated in glycolysis are potential substrates of TRIM21, further suggesting that TRIM21 as a regulator of glycolysis. The limitation of the current study is the lack of mechanistic insight into the signaling pathways resulting in TRIM21 upregulation in EAE. Future studies are needed to investigate whether TRIM21 is also elevated in other CNS diseases.

Although our study shed light on the role of PKM2 in astrocytes, whether PKM2 functions in a cell-specific manner or acts as a generalist warrants further studies. For example, microglia activation is a key step that contributes to CNS disorders such as multiple sclerosis and Alzheimer's disease (Long et al., 2024). Activated M1 microglial cells exhibit a metabolic switch toward aerobic glycolysis similar to that of

astrocytes. Thus, it is highly possible that PKM2 may also be involved in microglia metabolic change and activation. As such, PKM2 might be a novel therapeutic target for the treatment of CNS disease. However, further studies are needed to decipher the role of nuclear localized PKM2 in different cells under pathological conditions to provide a thorough understanding of the biological functions of PKM2.

In addition to identifying the contribution of TRIM21 to PKM2 nuclear translocation and TRIM21-PKM2 axis in promoting astrocyte glycolysis and proliferation, the therapeutic effect of TRIM21 in EAE was also tested. By using lentivirus with astrocyte-specific GFAP promoter, the knockdown of TRIM21 in astrocytes has been successfully achieved. This approach by using lentivirus to deliver shRNA into astrocytes has been previously reported by our group, in which shAct1 lentivirus showed potency for the treatment of EAE (Yan et al., 2012). In the presented study, we showed that blocking TRIM21 pathway effectively ameliorated disease severity of EAE, which is evidenced by the reduced inflammation, demyelination, activation of astrocytes and microglia. Moreover, we have tested the effect of blocking PKM2 nuclear translocation with TEPP-46. Although TEPP-46 has been shown to inhibit T cell activation in EAE development, its effect on CNS inflammation has not been explored (Angiari et al., 2020). We found that TEPP-46 treatment also reduced inflammatory infiltration and demyelination of the white matter. Moreover, a reduced activation of microglia and astrocytes was also observed in TEPP-46-treated group. Our in vivo results suggested that targeting TRIM21-PKM2 is a promising approach for clinical treatment of multiple sclerosis.

In conclusion, our study revealed that PKM2 nuclear translocation is the key mechanism accounting for glycolysis-dominant metabolic switch and proliferation of astrocytes. We propose a post-translational modification mechanism for the regulation of PKM2 nuclear translocation by the ubiquitin ligase TRIM21. From the perspective of metabolism, our study provides a rationale for targeting glycolysis metabolism to ameliorate astrocyte-mediated CNS diseases.

Materials and Methods

Animal experiments

Eight-week-old female C57BL/6 mice were obtained and kept in the animal center of Shaanxi Normal university. All experimental procedures complied with Committee for Research and Animal Ethics of Shaanxi Normal university. The induction of EAE model was conducted as previously described (Yan et al., 2012). For TEPP-46 treatment, mice were injected intraperitoneally (i.p) with 200 μl vehicle (5% DMSO, 30% PEG300, 5% Tween 80 and 60% ddH_2O) or 50 mg/kg TEPP-46 dissolved in vehicle every other day from day 0 to day 8 p.i. (post-immunization). All mice were divided into experimental groups randomly. All scoring processes were double-blinded. Mice were scored daily as follows: 0, no clinical symptoms; 1, paralyzed tail; 2, paralysis of one hind limb; 3, paralysis of two hind limbs; 4, paralysis of trunk; 5, death. Spinal cord tissue was collected at the onset (score 1; Day 7-17 p.i.), peak (score≥3; Day 14-24 p.i.) and chronic stages of EAE (score≥2; Day 21-26 p.i.).

In vivo injection of lentivirus

For in vivo injection of lentivirus, mice were anaesthetized and placed on a stereotaxic frame. 1×10^7 IU/mouse shTRIM21 or control virus was injected with microsyringe at the following coordinates: 2.0-mm lateral, 1.0-mm caudal to bregma, and 2.5 mm below the skull surface. 20 μl lentivirus was delivered at 1 μl/min. After each injection, the syringe was left for 10 min and then withdrawn slowly.

Isolation and culture of primary astrocytes

Neonatal mice were killed and neuronal tissues were dissociated using Neural

Tissue Dissociation Kit (Miltenyi Biotech, Auburn, CA) according to the manufacturer's instructions. Cell suspension was centrifuged at 800 g for 10 min. Subsequently, astrocytes were separated using anti-GLAST microbead kit (Miltenyi Biotech, Auburn, CA). Cells were seeded in 60 mm dishes and grown in DMEM supplemented with 10% FBS. Purity of astrocytes was >95% as determined by GFAP immunostaining.

Single-cell RNA sequencing

We prepared cells from mouse brain tissues by using adult brain dissociation kit (Miltenyi) according to the manufacturer's instruction. Briefly, cells with more than 90% viability were loaded onto the controller to generate single-cell gel bead emulsions. Single-cell RNA-seq libraries were prepared using version 3 Chromium Single Cell 3' Library (10×Genomics, https://www.10xgenomics.com/support/single-cell-gene-expression). Sequencing were performed on Illumina NovaSeq6000. We used Cell Ranger version 4.0.0 to process raw sequencing data, barcode processing and single-cell UMI (unique molecular index) counting. Sequencing data have been deposited into the Gene Expression Omnibus (GEO) under the accession number GSE263883.

Immunoprecipitation

Indicated antibodies (anti-PKM2, TRIM21, Flag, Myc and IgG) were incubated separately with Dynabeads M-270 Epoxy (Thermo Scientific) on a roller at 37°C overnight to generate antibody-conjugated beads. Cell samples were lysed with ice-cold extraction buffer (Thermo Scientific) containing protease inhibitors. Supernatants were incubated with appropriate antibody-conjugated magnetic beads on a roller at 4°C for 1 h. Precipitates were washed and subjected to subsequent western blotting analysis.

Lentivirus-mediated short hairpin RNA interference and overexpression

Mir-30 based lentiviral vector with GFAP promoter was constructed as previously described. XhoI and EcoRI sites were used for cloning small hairpin RNAs (shRNAs)(Yan et al., 2012).

Target sequences for shPKM2 were as follows: shPKM2-1:5′-GGAGCCTATG

AGTATCGAATG-3′, shPKM2-2:5′-GGAAAGAGTTGGCCGAGAAGA-3′, shPKM 2-3:5′-GCTCCCTCATTTACACCTTCT-3′, shControl: 5′- CCTAAGGTTAAGTCG CCCTCG-3′.

Primary astrocytes were cultured in six-well plates and infected with shTRIM21 or shControl. For overexpression of TRIM21, lentiviral vector with GFAP-promoter was used. TRIM21 cDNA was subcloned into lentivirus vector. Primary cultures were infected with LV-NC or LV-TRIM21.

Glucose consumption and lactate production assays

The indicated cells ($1x10^4$ per well) were seeded into 96-well plates and cultured for 24 h. Cells were starved for 12 h in serum-free DMEM medium supplemented with low glucose. With corresponding treatments, the supernatant was collected. Glucose consumption was determined using glucose oxidase method (Applygen Technologies, Beijing, China). The levels of lactate production were determined using lactate assay kit (Nanjing Jiancheng Bioengineering Institute, Nanjing, China). Glucose consumption and lactate production were normalized to cell numbers.

Immunofluorescence

For tissue immunofluorescence staining, cryosections were blocked with buffer containing 1% BSA and 0.3% Triton X-100 at room temperature (RT) for 1 h. Then, sections were incubated with primary antibodies anti-PKM2 (bs-0101R, Bioss), anti-GFAP (EM140707, Huabio), or anti-TRIM21 (12108-1-AP, Proteintech) overnight at 4°C. Then the Alexa Fluor 488 or Cy3-conjugated secondary antibodies (Zhuangzhibio, Xi'an, China) were applied at room temperature for 1 h. Cell nuclei were labeled with DAPI.

For cell immunochemistry, cells cultured on glass coverslips were fixed with 4% PFA for 10 min at RT, followed by permeabilization with 0.3% Triton X-100. Non-specific binding was blocked with buffer containing 3% BSA for 30 min at RT. Briefly, samples were then incubated with primary antibodies and secondary antibodies. DAPI was used to stain the nuclei. Tissues and cells were observed and images were acquired using an EVOS FL Auto 2 Cell image system (Invitrogen). The fluorescence intensity was measured by ImageJ.

Cell proliferation assays

Cells were plated at a density of 5 x 10^4 per well and cultured overnight. After treatment, the proliferation of astrocytes was assessed by an EdU-488 or EdU-594 cell proliferation detection kit (Beyotime, C0071S and C0078S). For Cell Counting Kit-8 analysis, cells were seeded separately in each 96-well plate and cultured for 24 h, 48 h and 72 h respectively. 1 h before the endpoint of incubation, 10 μl CCK-8 reagent was added, OD_{450nm} value was determined by Infinite F50 (Tecan) microplate reader.

Protein extraction and western blotting

Cells were lysed in RIPA buffer supplemented with proteinase inhibitor cocktail (Topscience, Shanghai, China). Whole cell lysates were obtained after centrifugation. Nuclear protein was extracted using Nuclear and cytoplasmic Extraction Kit (Solarbio, Beijing, China) according to the manufacturer's instructions. Protein concentrations were determined by using a BCA kit, and then subjected to western blotting. Protein samples were separated by SDS-PAGE and transferred onto PVDF membranes. After being blocked for 2h in 5% skim-milk buffer, membranes were incubated overnight at 4 °C with the following primary antibodies: antibodies against PKM2 (1:5000, 60268-1-Ig, Proteintech), phospho-c-myc (1:500, ET1609-64, Huabio), c-myc (1:1000, CPA1778, Cohesion Biosciences), LDHA (1:1000, ET1608-57, Huabio), STAT3 (1:5000, 60199-1-Ig, Proteintech), phospho-STAT3 (1:1000, bs-1658R, Bioss), phospho-p65 (1:1000, GB113882-100, Servicebio), p65 (1:1000, CPA2000, Cohesion Biosciences), phospho-IKK(1:1000, bs-3237R, Bioss), IKK (1:1000, GB11292-1-100, ServiceBio), Lamin (1:1000 CPA1693, Cohesion Biosciences), Tubulin (11224-1-AP, Proteintech), Flag (1:1000, AE004, Abclonal), Myc (1:3000, AE010, Abclonal), TRIM21 (1:1000, 12108-1-AP, Proteintech), and β-actin (1:2000, GB12001-100, ServiceBio). Membranes were then washed and probed with HRP conjugated secondary antibodies. Membranes were visualized with ECL detection system (Tanon 4600, Shanghai, China).

RNA extraction and qPCR

Total RNA was extracted with TRIzol and cDNA was synthesized by reverse transcription (DEEYEE, Shanghai, China). qPCR was performed by using 2×qPCR

SmArt Mix (DEEYEE, Shanghai, China) with StepOnePlus Real-time PCR system (Thermo Fisher). The fold-change data were obtained using the delta-delta Ct method (Livak and Schmittgen, 2001). Primers used in this study were listed in Supplementary Table S1.

Statistics

Data were analyzed with GraphPad Prism software (version 8.0). Differences between two groups were analyzed using two-tailed Student's t-test. Differences between more than two groups were determined by one-way ANOVA with Dunnett's post-hoc test. Mean clinical scores of animals were determined by two-way ANOVA analysis. A *P* value of< 0.05 indicated significant differences between groups.

Institutional Review Board Statement

The study was conducted in accordance with the Declaration of Helsinki, and approved by the Institutional Review Board of Shaanxi Normal university.

Acknowledgements

We thank Shanghai Bioprofile Biotechnology Co., Ltd for mass spectrometry and bioinformatics analysis.

Funding information

This work was supported by National Natural Science Foundation of China (No. 82071348), Natural Science Basic Research Program of Shaanxi (No. 2023-JC-JQ-64), Fundamental Research Funds for the Central University (No. GK202304034),

Author contributions

Conceptualization, L.T.Y; Methodology, L.T.Y, T.T.C, X.Z, Y.Y, Y.L.Z and Y.P.Y.;

Validation, L.T.Y and J. Z; Investigation, J.Z, C.Q.H, X.W.C, Y.X.X and W.T.H; scRNA-seq data analysis: Z.F; Data Curation, L.T.Y and J.Z; Writing – Original Draft Preparation, L.T.Y; Writing – Review & Editing, C.Q.H ; Supervision, Y.P.Y; Funding Acquisition, Y.P.Y and Y.Y.

Conflicts of interest

The authors declare no conflicts of interest.

Data availability

All data generated or analyzed during this study are included in the manuscript and supporting files.

References:

Afzal R, Dowling JK, McCoy CE. Impact of Exercise on Immunometabolism in Multiple Sclerosis. Journal of clinical medicine 2020;9(9):3038.

Angiari S, Runtsch MC, Sutton CE, Palsson-McDermott EM, Kelly B, Rana N, et al. Pharmacological Activation of Pyruvate Kinase M2 Inhibits CD4(+) T Cell Pathogenicity and Suppresses Autoimmunity. Cell metabolism 2020;31(2):391-405.e8.

Chen SJ, Wang YL, Kao JH, Wu SF, Lo WT, Wu CC, et al. Decoy receptor 3 ameliorates experimental autoimmune encephalomyelitis by directly counteracting local inflammation and downregulating Th17 cells. Molecular immunology 2009;47(2-3):567-74.

Chen X, Cao M, Wang P, Chu S, Li M, Hou P, et al. The emerging roles of TRIM21 in coordinating cancer metabolism, immunity and cancer treatment. Front Immunol 2022;13:968755.

Chen X, Li Z, Yong H, Wang W, Wang D, Chu S, et al. Trim21-mediated HIF-1α degradation attenuates aerobic glycolysis to inhibit renal cancer tumorigenesis

619 and metastasis. Cancer letters 2021;508:115-26.
620 Correale J, Farez MF. The Role of Astrocytes in Multiple Sclerosis Progression.
621 Frontiers in neurology 2015;6:180.
622 das Neves SP, Sousa JC, Sousa N, Cerqueira JJ, Marques F. Altered astrocytic
623 function in experimental neuroinflammation and multiple sclerosis. Glia
624 2021;69(6):1341-68.
625 Dhanesha N, Patel RB. PKM2 promotes neutrophil activation and cerebral
626 thromboinflammation: therapeutic implications for ischemic stroke. Blood
627 2022;139(8):1234-45.
628 Gu M, Tan M, Zhou L, Sun X, Lu Q, Wang M, et al. Protein phosphatase 2Acα
629 modulates fatty acid oxidation and glycolysis to determine tubular cell fate
630 and kidney injury. Kidney international 2022;102(2):321-36.
631 Kozela E, Juknat A, Kaushansky N, Ben-Nun A, Coppola G, Vogel Z. Cannabidiol, a
632 non-psychoactive cannabinoid, leads to EGR2-dependent anergy in activated
633 encephalitogenic T cells. Journal of neuroinflammation 2015;12:52-.
634 Kuhlmann T, Moccia M, Coetzee T, Cohen JA, Correale J, Graves J, et al. Multiple
635 sclerosis progression: time for a new mechanism-driven framework. The
636 Lancet Neurology 2023;22(1):78-88.
637 Lee H-G, Lee J-H, Flausino LE, Quintana FJ. Neuroinflammation: An astrocyte
638 perspective. Science translational medicine 2023;15(721):eadi7828.
639 Lee Y-B, Min JK, Kim J-G, Cap KC, Islam R, Hossain AJ, et al. Multiple functions of
640 pyruvate kinase M2 in various cell types. Journal of cellular physiology
641 2022;237(1):128-48.
642 Li M, Lu W, Meng Y, Zhang W, Wang F, Sun L, et al. Tetrahydroxy Stilbene
643 Glucoside Alleviates Ischemic Stroke by Regulating Conformation-Dependent
644 Intracellular Distribution of PKM2 for M2 Macrophage Polarization. Journal
645 of agricultural and food chemistry 2022;70(49):15449-63.
646 Liu C, Liu C, Fu R. Research progress on the role of PKM2 in the immune response.
647 Front Immunol 2022;13:936967.
648 Livak KJ, Schmittgen TD. Analysis of relative gene expression data using real-time

649 quantitative PCR and the 2(-Delta Delta C(T)) Method. Methods
650 2001;25(4):402-8.
651 Long Y, Li X-q, Deng J, Ye Q-b, Li D, Ma Y, et al. Modulating the polarization
652 phenotype of microglia – A valuable strategy for central nervous system
653 diseases. Ageing research reviews 2024;93:102160.
654 Lorenzana-Carrillo MA, Gopal K, Byrne NJ, Tejay S, Saleme B, Das SK, et al.
655 TRIM35-mediated degradation of nuclear PKM2 destabilizes GATA4/6 and
656 induces P53 in cardiomyocytes to promote heart failure. Science translational
657 medicine 2022;14(669):eabm3565.
658 Nijland PG, Molenaar RJ, van der Pol SM, van der Valk P, van Noorden CJ, de Vries
659 HE, et al. Differential expression of glucose-metabolizing enzymes in multiple
660 sclerosis lesions. Acta neuropathologica communications 2015;3:79.
661 Patani R, Hardingham GE, Liddelow SA. Functional roles of reactive astrocytes in
662 neuroinflammation and neurodegeneration. Nature reviews Neurology
663 2023;19(7):395-409.
664 Shang Y, He J, Wang Y, Feng Q, Zhang Y, Guo J, et al. CHIP/Stub1 regulates the
665 Warburg effect by promoting degradation of PKM2 in ovarian carcinoma.
666 Oncogene 2017;36(29):4191-200.
667 Tang Y, Jia Y, Fan L, Liu H, Zhou Y, Wang M, et al. MFN2 Prevents Neointimal
668 Hyperplasia in Vein Grafts via Destabilizing PFK1. Circulation research
669 2022;130(11):e26-e43.
670 Traxler L, Herdy JR, Stefanoni D, Eichhorner S, Pelucchi S, Szücs A, et al.
671 Warburg-like metabolic transformation underlies neuronal degeneration in
672 sporadic Alzheimer's disease. Cell metabolism 2022;34(9):1248-63.e6.
673 Vaupel P, Multhoff G. Revisiting the Warburg effect: historical dogma versus current
674 understanding. The Journal of physiology 2021;599(6):1745-57.
675 Verkhratsky A, Butt A, Li B, Illes P, Zorec R, Semyanov A, et al. Astrocytes in human
676 central nervous system diseases: a frontier for new therapies. Signal
677 transduction and targeted therapy 2023;8(1):396.
678 Viana R, Lujan P, Sanz P. The laforin/malin E3-ubiquitin ligase complex ubiquitinates

679 pyruvate kinase M1/M2. BMC Biochem 2015;16:24.
680 Wei X, Jin XH, Meng XW, Hua J, Ji FH, Wang LN, et al. Platelet-rich plasma
681 improves chronic inflammatory pain by inhibiting PKM2-mediated aerobic
682 glycolysis in astrocytes. Annals of translational medicine 2020;8(21):1456.
683 Wu H, Guo X, Jiao Y, Wu Z, Lv Q. TRIM35 ubiquitination regulates the expression of
684 PKM2 tetramer and dimer and affects the malignant behaviour of breast
685 cancer by regulating the Warburg effect. International journal of oncology
686 2022;61(6):144.
687 Xiong XY, Tang Y, Yang QW. Metabolic changes favor the activity and heterogeneity
688 of reactive astrocytes. Trends in endocrinology and metabolism: TEM
689 2022;33(6):390-400.
690 Yan Y, Ding X, Li K, Ciric B, Wu S, Xu H, et al. CNS-specific therapy for ongoing
691 EAE by silencing IL-17 pathway in astrocytes. Molecular therapy : the journal
692 of the American Society of Gene Therapy 2012;20(7):1338-48.
693 Yang L, Jin L, Ke Y, Fan X, Zhang T, Zhang C, et al. E3 Ligase Trim21 Ubiquitylates
694 and Stabilizes Keratin 17 to Induce STAT3 Activation in Psoriasis. Journal of
695 Investigative Dermatology 2018;138(12):2568-77.
696 Yang L, Zhang T, Zhang C, Xiao C, Bai X, Wang G. Upregulated E3 ligase tripartite
697 motif-containing protein 21 in psoriatic epidermis ubiquitylates nuclear factor-
698 κB p65 subunit and promotes inflammation in keratinocytes*. British Journal
699 of Dermatology 2021;184(1):111-22.
700 Yang W, Zheng Y, Xia Y, Ji H, Chen X, Guo F, et al. ERK1/2-dependent
701 phosphorylation and nuclear translocation of PKM2 promotes the Warburg
702 effect. Nature cell biology 2012;14(12):1295-304.
703 Zhang J, Feng G, Bao G, Xu G, Sun Y, Li W, et al. Nuclear translocation of PKM2
704 modulates astrocyte proliferation via p27 and -catenin pathway after spinal
705 cord injury. Cell Cycle 2015;14(16):2609-18.
706 Zhou Q, Yin Y, Yu M, Gao D, Sun J, Yang Z, et al. GTPBP4 promotes hepatocellular
707 carcinoma progression and metastasis via the PKM2 dependent glucose
708 metabolism. Redox biology 2022;56:102458.

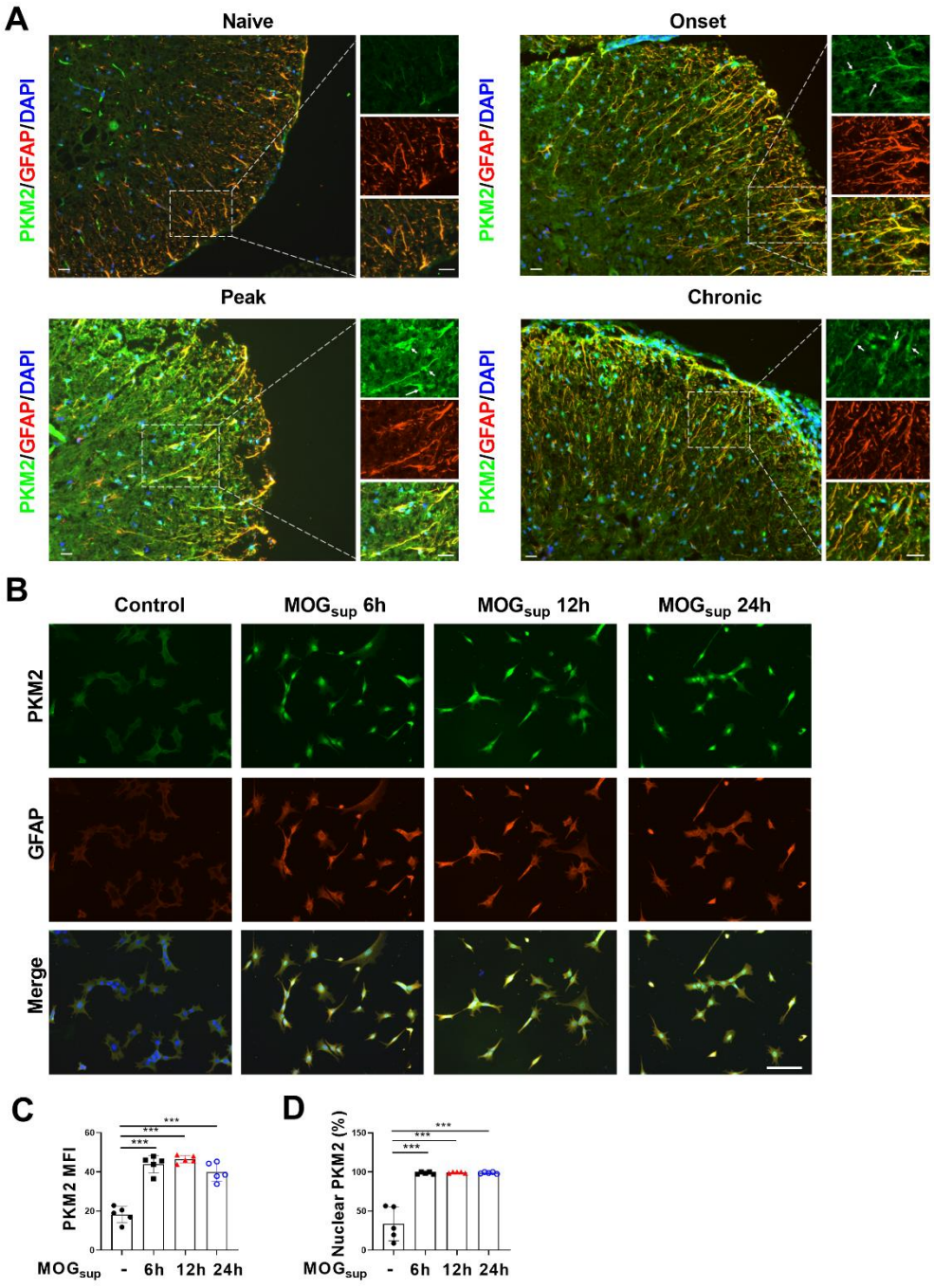

Figure 1. Nuclear translocation of PKM2 in astrocytes of EAE mice. (A) Immunofluorescence staining of PKM2 with GFAP (astrocyte marker) in spinal cord of control mice and MOG35–55-induced EAE mice. Disease onset (dpi 7–17), peak (dpi 14–24) and chronic (dpi 21–26) were defined dependent on the EAE course. Scale bar: 20 μm. While arrows indicated nuclear PKM2. (B) Immunofluorescence staining of PKM2 with GFAP in primary astrocytes cultured with splenocytes supernatants of MOG35–55-induced EAE mice (MOGsup) for different time points (6 h, 12 h and 24 h). Scale bar: 100 μm. (C) Mean fluorescence intensity of PKM2 and nuclear PKM2 ratio (D) in different groups of (B) were calculated. Fight fields of views per group were included in the analysis. Data are represented as mean ± SEM. ***P<0.001. SEM, standard error of the mean.

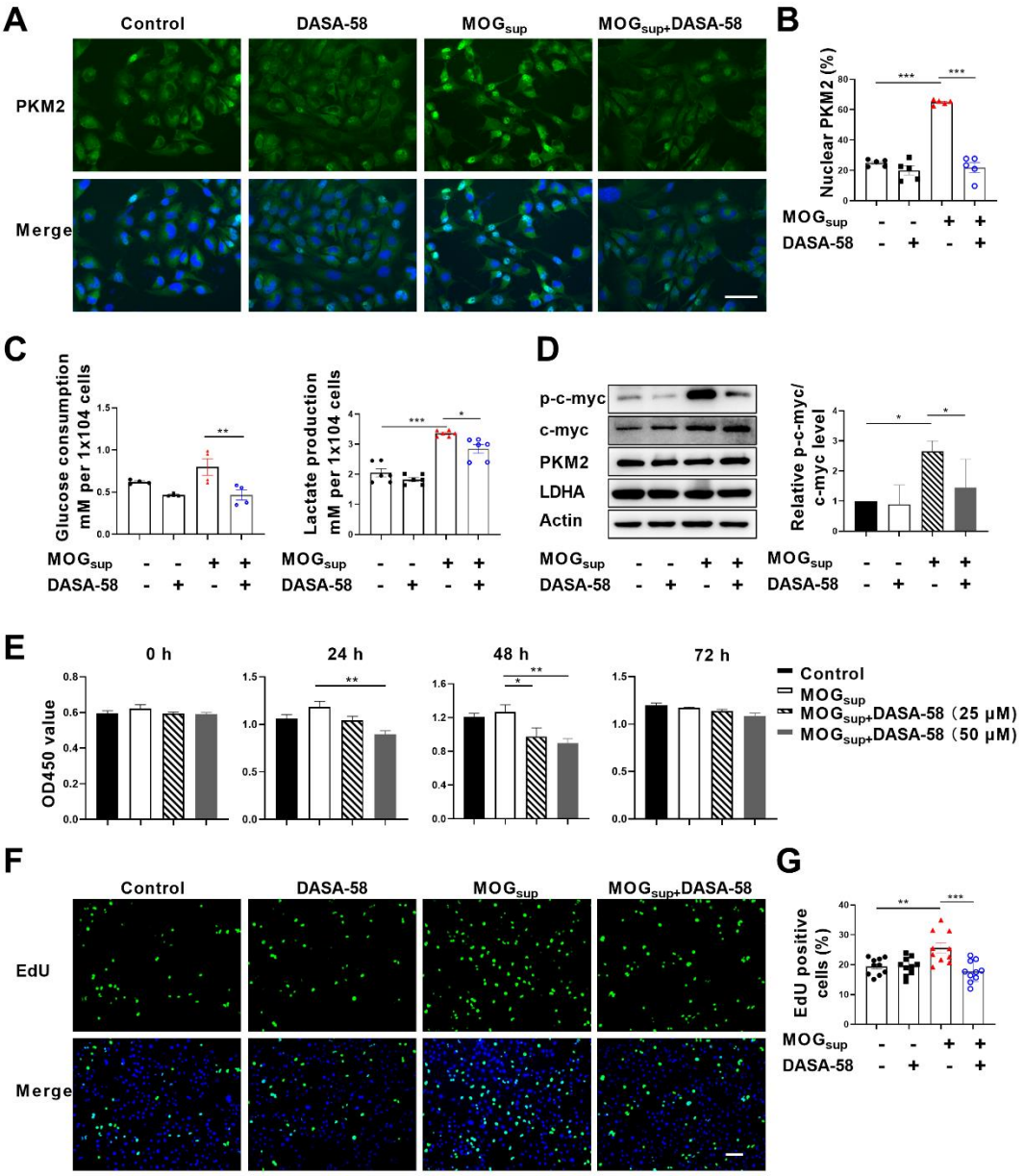

Figure 2. Prevention of PKM2 nuclear transport reduced the glycolysis and proliferation of primary astrocytes. (A) Verification of DASA-58 effect on the inhibition of PKM2 nuclear transport by immunofluorescence. Primary astrocytes were pretreated with 50 μM DASA-58 for 30 min and stimulated with MOG_{sup} for 12h. Scale bar: 50 μm. (B) Nuclear ratio of PKM2 in each group was calculated. Five fields of views per group were included in the analysis. (C) Glycolysis level of astrocytes in each group was assessed by lactate production (N=5) and glucose consumption (N=4) assays. (D) Effect of DASA-58 on protein levels of glycolytic enzymes p-c-myc, LDHA and PKM2 were measured by western blotting. (E) Proliferation of astrocytes were measured by CCK8. N=5. (F) Proliferation of astrocytes were measured by EdU assays. (G) EdU positive cells in each group was calculated from ten fields of views per group. Scale bar: 100 μm. The blot is representative of three independent experiments. Data are represented as mean ± SEM. **P*<0.05; ***P*<0.01; ****P*<0.001. SEM, standard error of the mean.

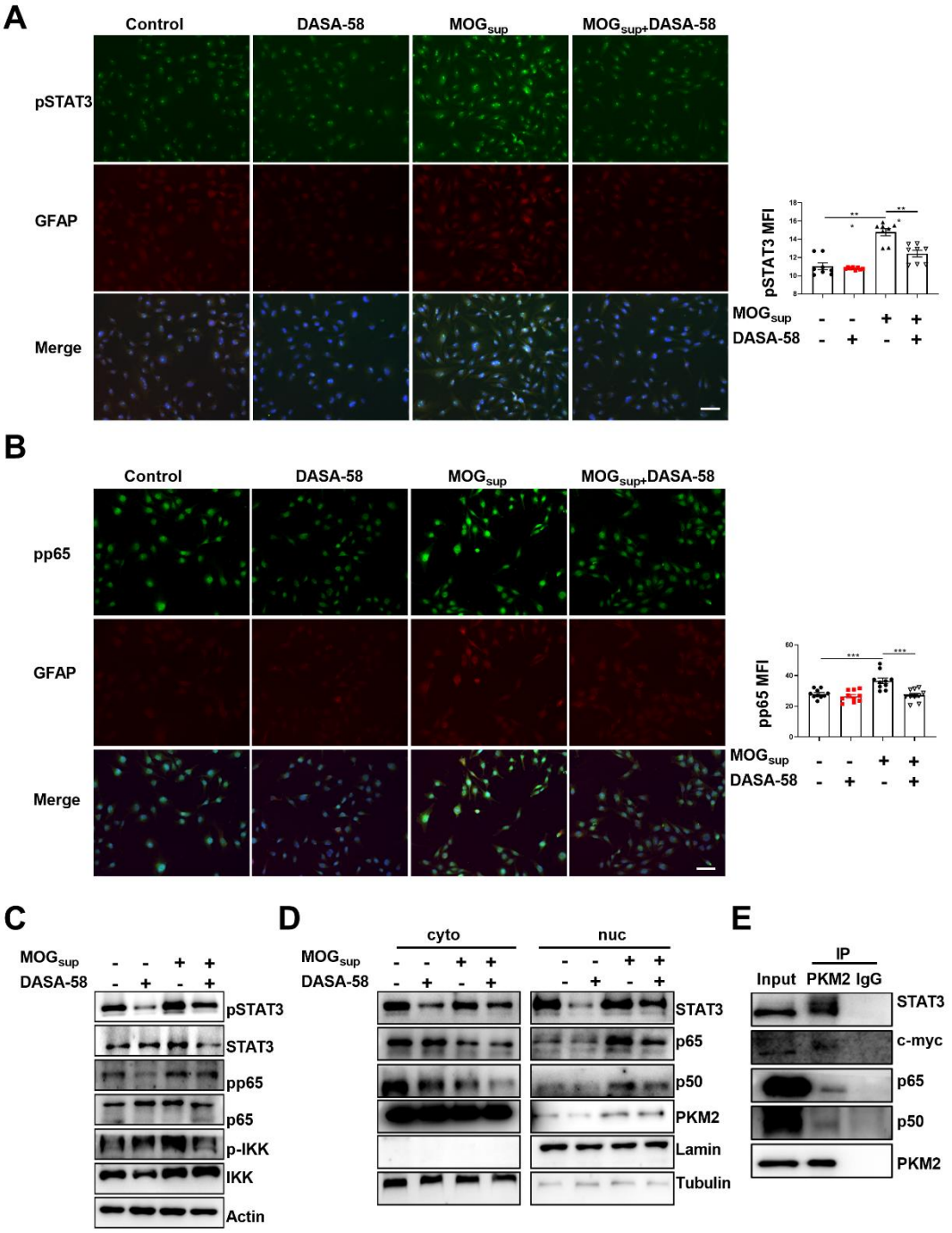

Figure 3. PKM2 interacted with STAT3 and NF-κB and promoted their activation in astrocytes. (A-B) Immunofluorescence staining of phospho-STAT3 (A) or phospho-p65 (B) with GFAP in astrocytes. Primary astrocytes were pretreated with 50 μM DASA-58 for 30 min and stimulated with MOG_{sup} for 12h. Scale bar: 100 μm. (C) Western blotting analysis showed that DASA-58 inhibited the activation of NF-κB and STAT3 induced by MOG_{sup} stimulation. (D) Nuclear-cytoplasmic protein extraction analysis showed the reduced nuclear fraction of STAT3 and p50/p65 upon DASA-58 treatment. (E) Immunoprecipitation demonstrated the interaction between PKM2 and STAT3, c-myc and p50/p65 subunits of NF-κB. Data are represented as mean ± SEM. $^{**}P<0.01$; $^{***}P<0.001$. SEM, standard error of the mean.

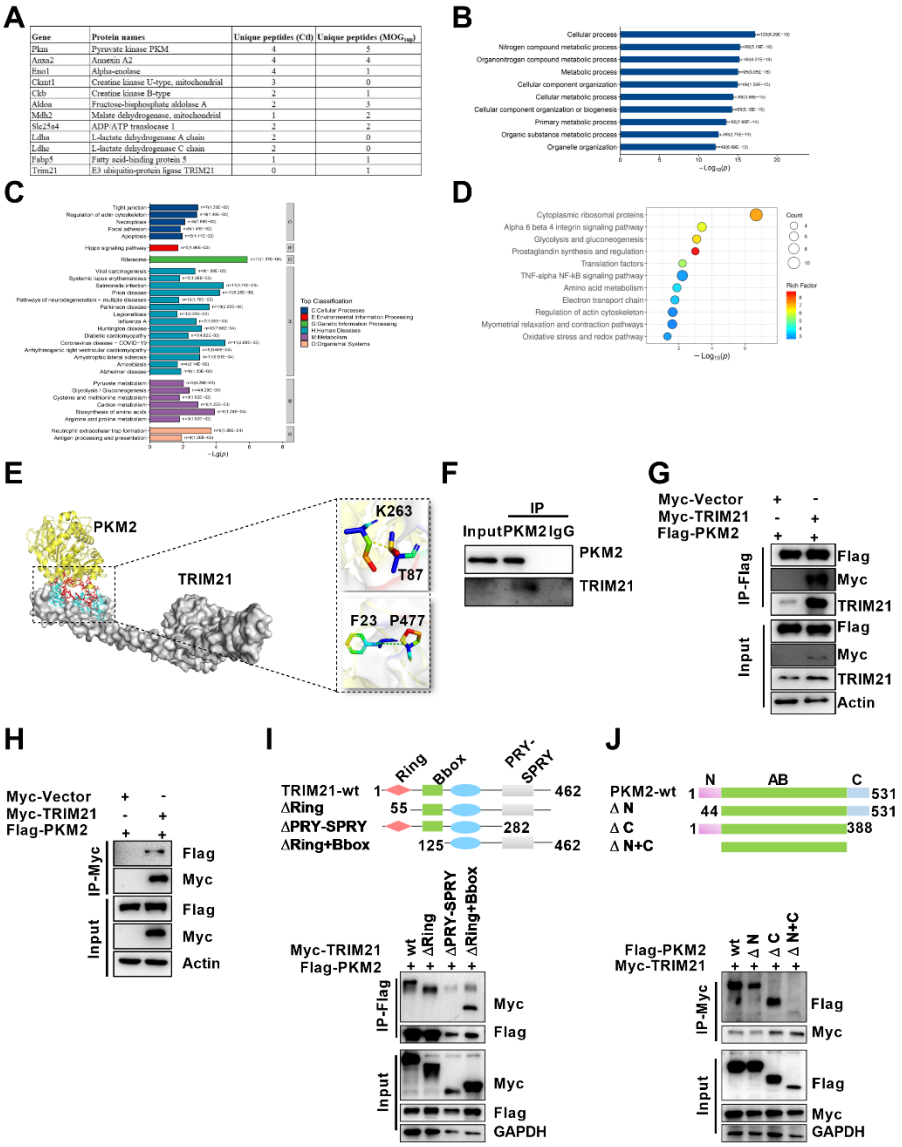

Figure 4. Identification of interaction between E3 ligase TRIM21 and PKM2 in astrocytes. (A) Mass spectrometry (MS) showed the list of metabolic-related proteins that potentially interact with PKM2 in primary astrocytes. TRIM21 was identified to interact with PKM2. (B-D) Biological process of GO term (B), KEGG pathway (C) and Wikipathway (D) analysis of proteins identified by MS. (E) Interaction between PKM2 and TRIM21 was predicted with molecular docking and showed by PyMol. The hydrogen bonds were formed between Phe23, Thr87 of TRIM21 and Pro477, Lys 263 of PKM2. (F) Immunoprecipitation showed the interaction between endogenous PKM2 and TRIM21 in primary astrocyte. (G-H) Primary astrocytes were transfected with Myc-tagged TRIM21 and Flag-tagged PKM2, immunoprecipitation with anti-Flag (G) or anti-Myc (H) showed the exogenous binding between PKM2 and TRIM21 in astrocytes. (I) Full-length TRIM21 and a series of TRIM21 mutants with deletion (Δ) of various domains (top panel). 293 T cells were co-transfected with Flag-PKM2 and WT Myc-TRIM21 or their truncation mutants for 48 h. Immunoprecipitation was performed. (J) Full-length PKM2 and a series of PKM2 mutants with deletion (Δ) of various domains (top panel). 293 T cells were co-transfected

with Myc-TRIM21 and WT Flag-PKM2 or their truncation mutants for 48 h. Immunoprecipitation was performed.

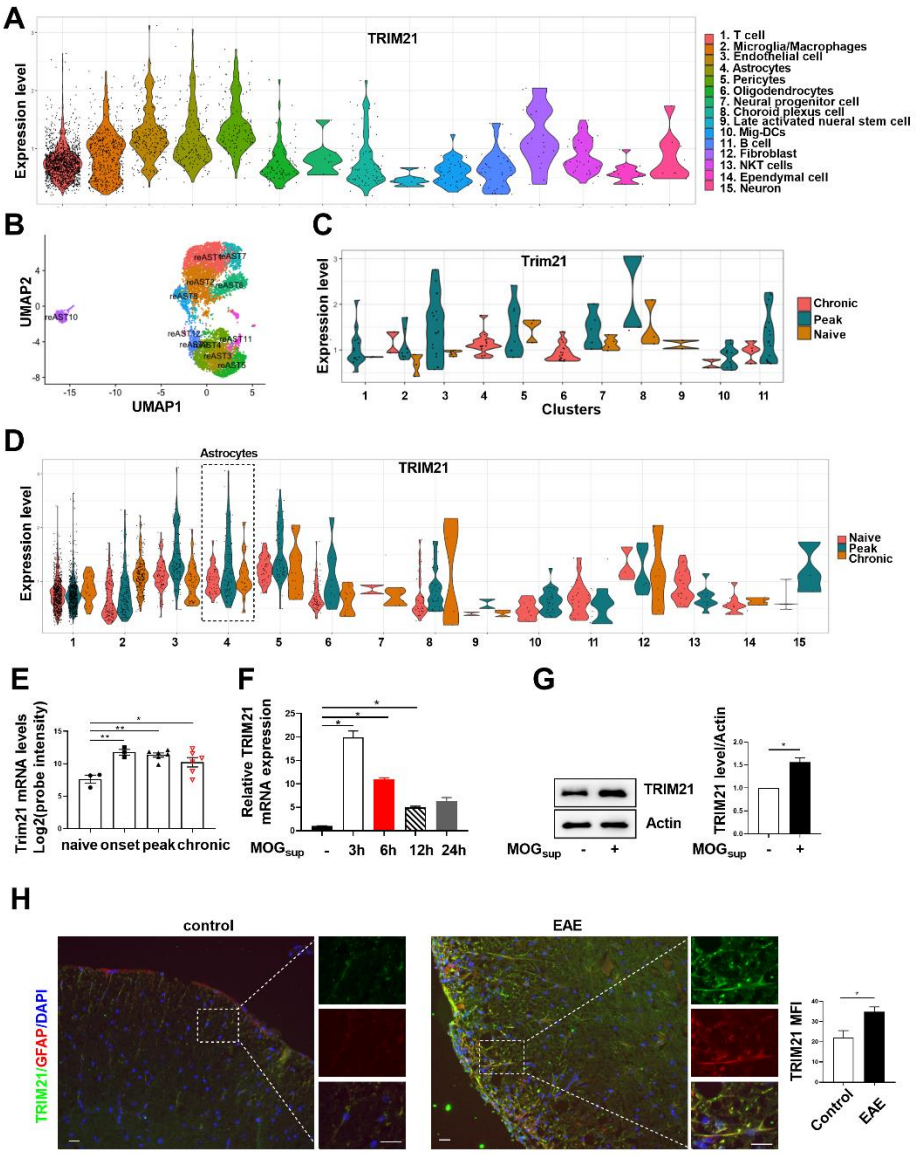

Figure 5. TRIM21 expression is upregulated in astrocytes of EAE mice. (A-D) Single-cell RNA-seq profiles from naive and EAE mice (peak and chronic phase) CNS tissues. Naive (n=2); peak (n=3); chronic (n=2). (A) Violin plots displaying the expression of TRIM21 across the cell types identified. (B) UMAP representation of 12 clusters generated from sub-clustering of astrocytes. (C) Violin plots displaying the expression of TRIM21 at peak, chronic phases from EAE and naive mice in subclusters of astrocytes. (D) Violin plots displaying the expression of TRIM21 in different phases of EAE and naive mice across the cell types identified. Expression of TRIM21 was shown to be elevated in EAE mice (peak and chronic) compared with naive mice. (E) Analysis of TRIM21 mRNA expression in astrocytes from spinal cord during three stages (onset, peak, and chronic) of EAE and naive mice from GEO dataset (GSE136358). (F) Primary astrocytes were treated with or without MOG_{sup} for different time points. Analysis of TRIM21 expression by qPCR. (G) Western blotting analysis of TRIM21 protein expression in non-treated or MOG_{sup}-treated astrocytes. (H) Immunofluorescence staining showed the upregulated

expression of TRIM21 in astrocytes (marker: GFAP) of EAE mice. Scale bar: 20 μm. Data are represented as mean ± SEM. *P<0.05; **P<0.01. SEM, standard error of the mean.

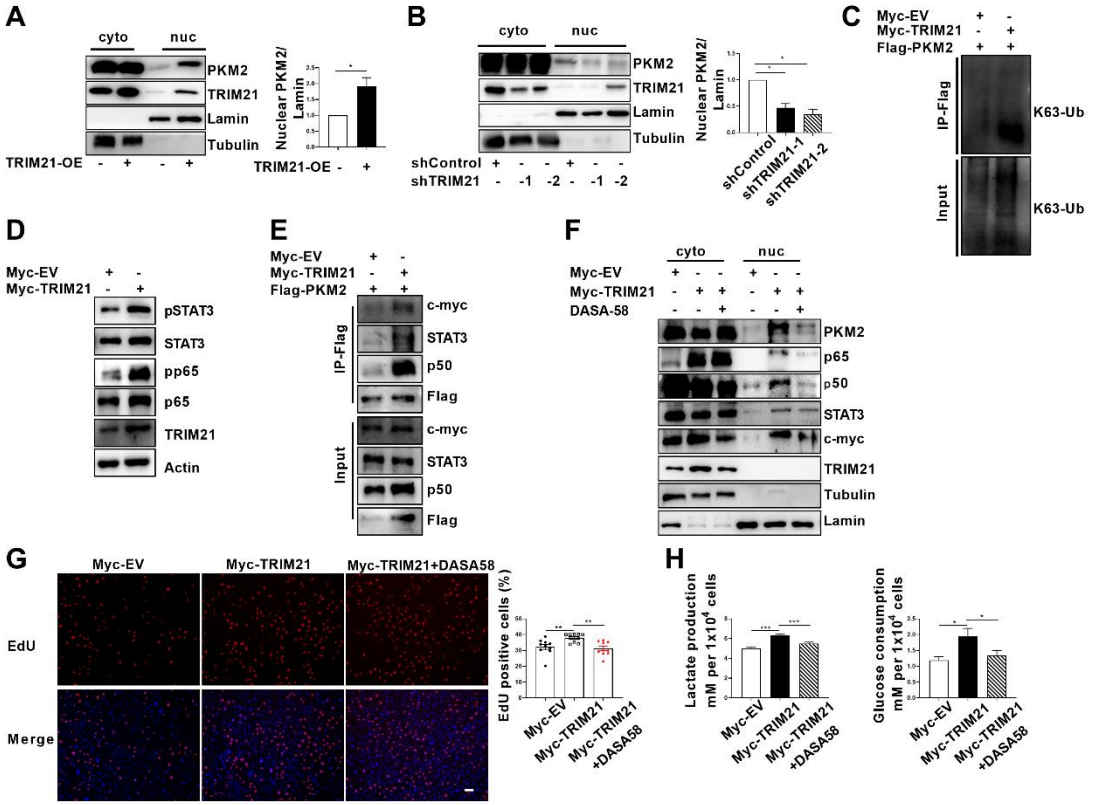

Figure 6. TRIM21-induced nuclear transport of PKM2 promoted glycolysis and proliferation of astrocytes. (A) Overexpression of TRIM21 promoted nuclear translocation of PKM2. (B) TRIM21 was silenced in primary astrocytes using two independent short hairpin RNAs. Nuclear-cytoplasmic fraction analysis showed that knockdown of TRIM21 decreased nuclear ratio of PKM2. (C) Immunoprecipitation showed that TRIM21 promoted the K63-linked ubiquitination of PKM2. (D) Western blotting analysis of STAT3 and NF-κB activation in control or TRIM21-overexpressed astrocytes. (E) Immunoprecipitation showed that TRIM21 promoted the interaction between PKM2 and its interacting proteins c-myc, STAT3 and p50. (F) Prevention of PKM2 nuclear import with DASA-58 (50 μM) reduced the nuclear retention of NF-κB subunits and STAT3 in TRIM21-overexpressed astrocytes. (G) EdU analysis of cell proliferation in TRIM21-overexpressed, DASA-58 treated TRIM21-overexpressed cells and control astrocytes. Scale bar: 100 μm. (H) Glycolysis of astrocytes were measured in TRIM21-overexpressed, DASA-58 treated TRIM21-OE cells and control astrocytes. EV: empty vector. Data are represented as mean ± SEM. *P<0.05; **P<0.01; ***P<0.001. SEM, standard error of the mean.

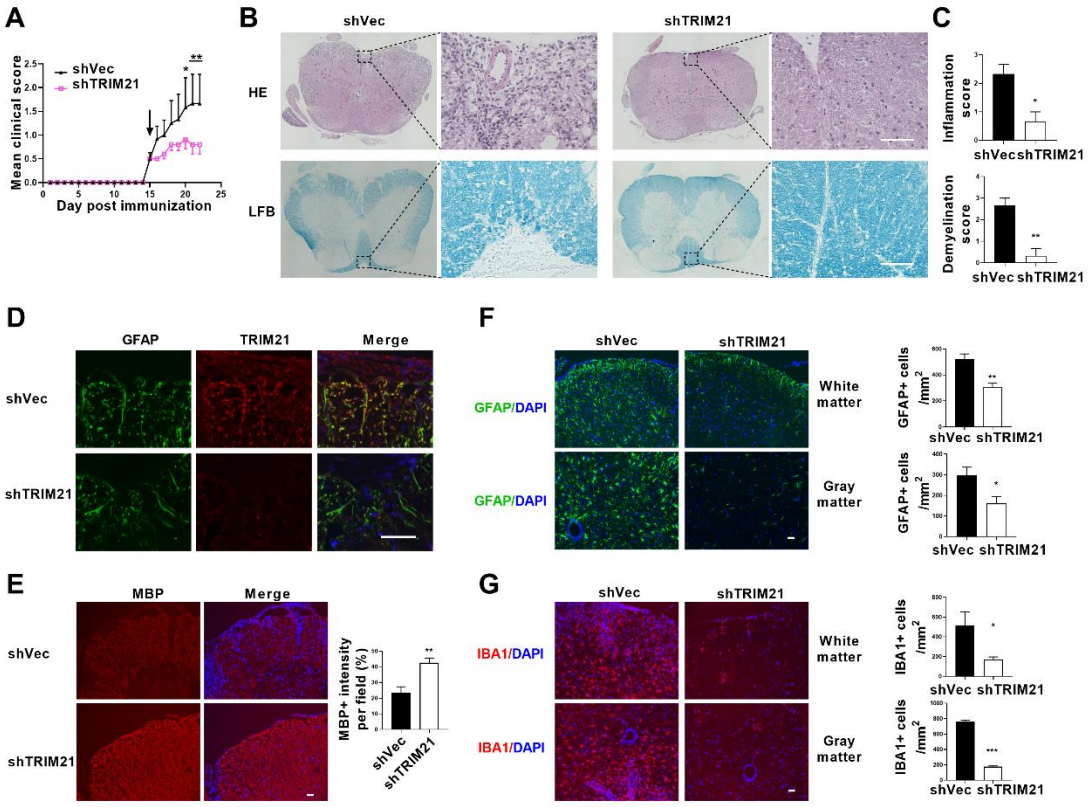

Figure 7. Intracerebroventricular injection of shTRIM21 ameliorates disease severity of Experimental Autoimmune Encephalomyelitis (EAE). C57BL/6 mice were injected i.c.v with $1x10^7$ IU shTRIM21 or control lentivirus (shVec) 15 days p.i. (onset). Mice were sacrificed at day 22 p.i. and spinal cords were harvested. (A) Disease was scored daily on a 0 to 5 scale. N=5 to 6 mice in each group. (B) Spinal cord sections were stained for markers of inflammation by hematoxylin and eosin (H&E) and demyelination by Luxol fast blue (LFB), respectively. (C) Scoring of inflammation (H&E) and demyelination (LFB) on a 0-3 scale. (D) TRIM21 expression in spinal cord of mice from shVec and shTRIM21 group was measured by immunofluorescence. (E) Demyelination in each group was assessed by MBP staining. MBP intensity was measured in the white matter of the spinal cord using Image-Pro. (F-G) Immunostaining of GFAP (F) and IBA1 (G) on spinal cord sections of shVec and shTRIM21-treated EAE mice. White matter and gray matter are shown as representative images. Quantification of GFAP positive cells/mm^2, IBA1 positive cells/mm^2 in both the white matter and gray matter. The measured areas included 3 to 5 fields per group. i.c.v., intracerebroventricular; p.i., postimmunization. Scale bar: 50 μm. Data are represented as mean ± SEM. **P*<0.05; ***P*<0.01; ****P*<0.001, as determined by two-way ANOVA analysis (A) or unpaired Student's t test (C, F-G).

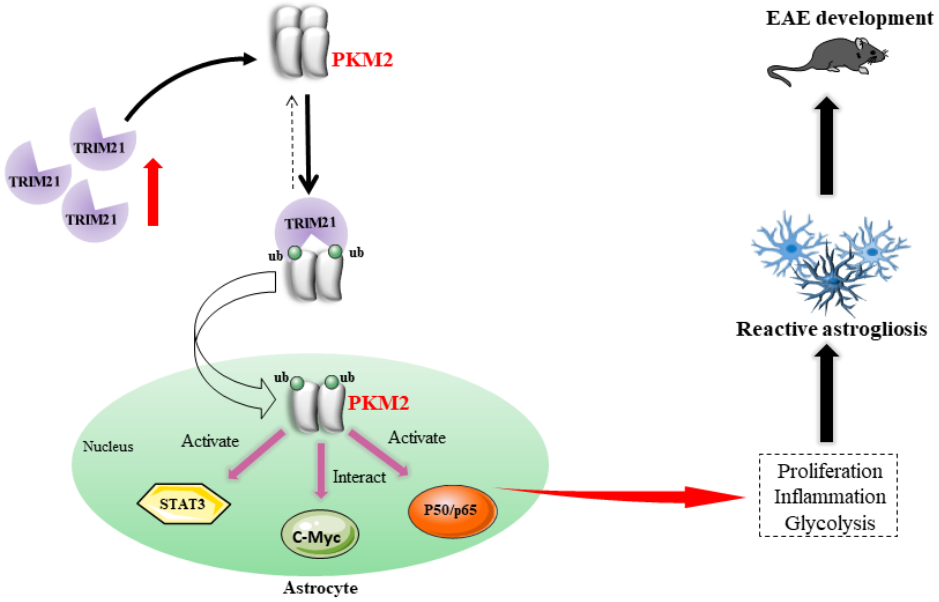

Figure 8. Schematic proposal of nuclear translocation of PKM2 in astrocytes of EAE. In astrocyte of EAE mice, TRIM21 expression is upregulated. E3 ubiquitin ligase TRIM21 ubiquitylates PKM2 and promotes its nuclear translocation, nuclear PKM2 activated STAT3 and NF-κB pathways and interact with c-Myc to enhance glycolysis and proliferation in astrocytes. Thus, TRIM21-PKM2 pathway exerts a potential role in activating astrocytes and inducing EAE development.

Supplementary Table S1. Primers used in this study.

Name	Primer sequences (5'-3' orientation)
PKM2	Forward: GCCGCCTGGACATTGACTC
	Reverse: CCATGAGAGAAATTCAGCCGAG
TRIM21	Forward: GGGAGGAGGTCACCTGTTCTA
	Reverse: GGCACTCGGGACATGAACTG
IL-6	Forward: GCTGGAGTCACAGAAGGAGTGGC
	Reverse: GGCATAACGCACTAGGTTTGCCG
IL-1β	Forward: CACTACAGGCTCCGAGATGAACAAC
	Reverse: TGTCGTTGCTTGGTTCTCCTTGTAC
TNF-α	Forward: CCTGTAGCCCACGTCGTAG
	Reverse: GGGAGTAGACAAGGTACAACCC
Cyclin D1	Forward: AAGTGCGTGCAGAAGGAGATTGT
	Reverse: GGATAGAGTTGTCAGTGTAGATGC
GAPDH	Forward: AGGTCGGTGTGAACGGATTTG
	Reverse: TGTAGACCATGTAGTTGAGGTCA

Supplementary Figures

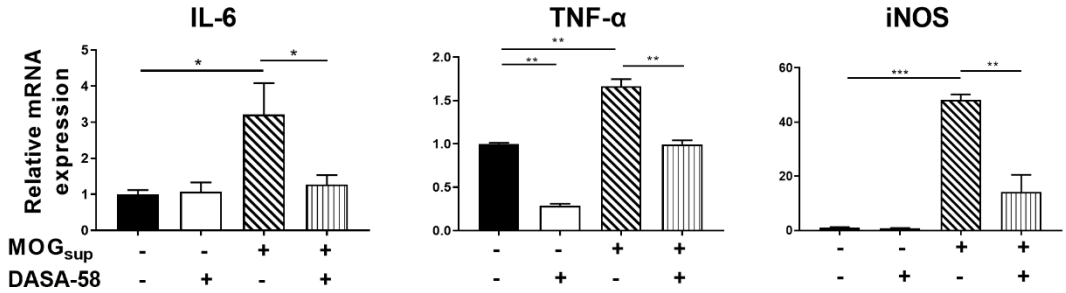

Figure S1. qPCR analysis of mRNA levels of inflammatory cytokines. Primary astrocytes were pretreated with 50 μM DASA-58 for 30 min and stimulated with MOG_{sup} for 12h. Data are represented as mean ± SEM. **P*<0.05; ***P*<0.01; ****P*<0.001. SEM, standard error of the mean.

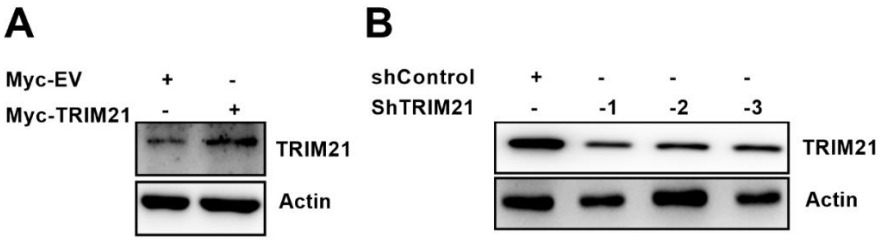

Figure S2. Verification of TRIM21 overexpression and knockdown efficiency. (A) Overexpression of TRIM21 was verified by western blotting analysis. (B) Western Blotting analysis of TRIM21 knockdown efficiency. Sh: short hairpin; EV: empty vector.

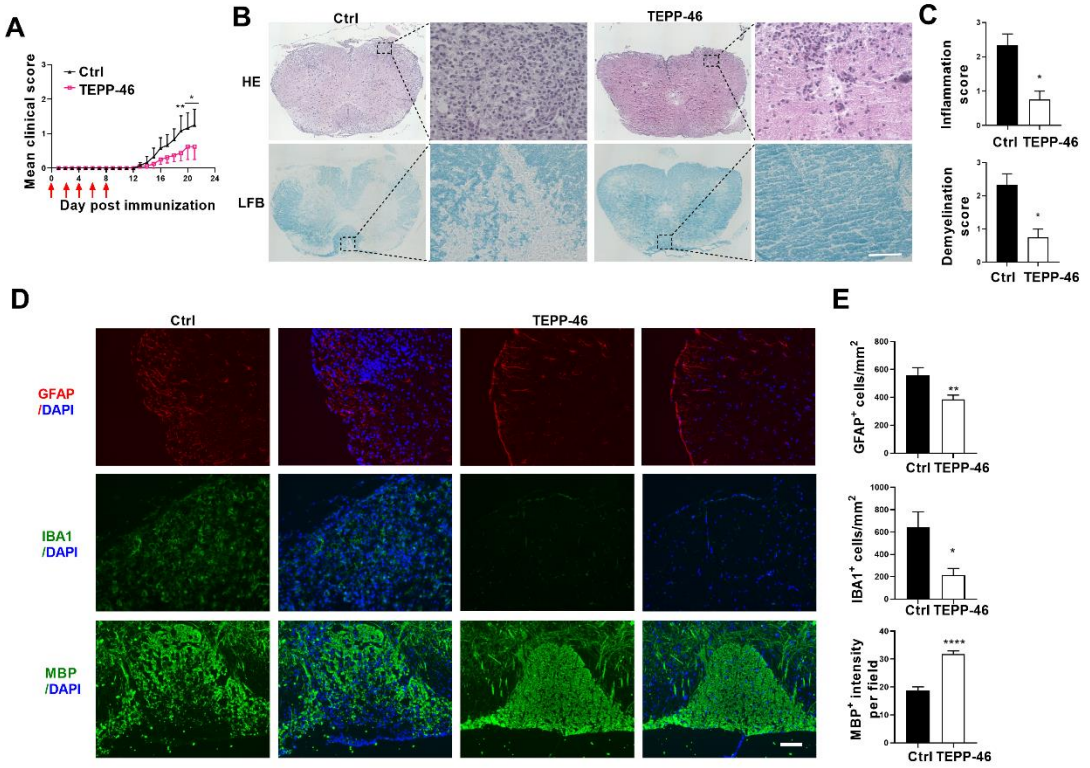

Figure S3. i.p. injection of TEPP-46 alleviated the development of Experimental Autoimmune Encephalomyelitis (EAE). C57BL/6 mice were i.p injected with 200 µl vehicle or 50 mg/kg TEPP-46 dissolved in vehicle every other day from day 0 to day 8 p.i.. Mice were sacrificed at day 21 p.i. and spinal cords were harvested. (A) Disease was scored daily on a 0 to 5 scale. N=6 to 8 mice in each group. (B) Spinal cord sections were stained for markers of inflammation by hematoxylin and eosin (H&E) and demyelination by Luxol fast blue (LFB), respectively. Scale bar: 50 µm. (C) Scoring of inflammation (H&E) and demyelination (LFB) on a 0-3 scale. (D) Immunostaining of GFAP, IBA1 and MBP on spinal cord sections of TEPP-46- or vehicle-treated EAE mice. (E) Quantification of GFAP positive cells/mm2, IBA1 positive cells/mm2 in the white matter of the spinal cord. MBP intensity was measured in the white matter of the spinal cord using Image-Pro. The measured areas included 3 to 5 fields per group. i.p., intraperitoneally; p.i., postimmunization; Scale bar: 100 µm. Data are represented as mean ± SEM. *P<0.05; **P<0.01; ***P<0.001, as determined by two-way ANOVA analysis (A) or unpaired Student's t test (C, E).

886